applied sciences

MDPI

Article

Maximum Power Extraction from a Standalone Photo Voltaic System via Neuro-Adaptive Arbitrary Order Sliding Mode Control Strategy with High Gain Differentiation

Muhammad Bilal Anjum [1], Qudrat Khan [2], Safeer Ullah [1], Ghulam Hafeez [1,3,*], Adnan Fida [1], Jamshed Iqbal [4] and Fahad R. Albogamy [5]

[1] Department of Electrical and Computer Engineering, COMSATS University Islamabad, Islamabad 45550, Pakistan; engrbilal93@gmail.com (M.B.A.); imdrsafeer@gmail.com (S.U.); adnan_fida@comsats.edu.pk (A.F.)
[2] Centre for Advanced Studies in Telecommunications (CAST), COMSATS University Islamabad, Islamabad Campus, Islamabad 45550, Pakistan; qudratullah@comsats.edu.pk
[3] Department of Electrical Engineering, University of Engineering and Technology, Mardan 23200, Pakistan
[4] Department of Computer Science and Technology, Faculty of Science and Engineering, University of Hull, Hull HU6 7RX, UK; j.iqbal@hull.ac.uk
[5] Computer Sciences Program, Turabah University College, Taif University, P.O. Box 11099, Taif 21944, Saudi Arabia; f.alhammdani@tu.edu.sa
* Correspondence: ghulamhafeez393@gmail.com or ghulamhafeez@uetmardan.edu.pk; Tel.: +92-300-5003574 or +92-348-8818497

Abstract: In this work, a photovoltaic (PV) system integrated with a non-inverting DC-DC buck-boost converter to extract maximum power under varying environmental conditions such as irradiance and temperature is considered. In order to extract maximum power (via maximum power transfer theorem), a robust nonlinear arbitrary order sliding mode-based control is designed for tracking the desired reference, which is generated via feed forward neural networks (FFNN). The proposed control law utilizes some states of the system, which are estimated via the use of a high gain differentiator and a famous flatness property of nonlinear systems. This synthetic control strategy is named neuro-adaptive arbitrary order sliding mode control (NAAOSMC). The overall closed-loop stability is discussed in detail and simulations are carried out in Simulink environment of MATLAB to endorse effectiveness of the developed synthetic control strategy. Finally, comparison of the developed controller with the backstepping controller is done, which ensures the performance in terms of maximum power extraction, steady-state error and more robustness against sudden variations in atmospheric conditions.

Keywords: arbitrary-order sliding-mode control; closed-loop stability; feed-forward neural network; high-gain differentiator; maximum power extraction; photovoltaic system

check for updates

Citation: Anjum, M.B.; Khan, Q.; Ullah, S.; Hafeez, G.; Fida, A.; Iqbal, J.; Albogamy, F.R. Maximum Power Extraction from a Standalone Photo Voltaic System via Neuro-Adaptive Arbitrary Order Sliding Mode Control Strategy with High Gain Differentiation. *Appl. Sci.* **2022**, *12*, 2773. https://doi.org/10.3390/app12062773

Academic Editor: Vincenza Brancato

Received: 3 January 2022
Accepted: 28 January 2022
Published: 8 March 2022

1. Introduction

Entire world electricity demand is rising continuously, which motivates the researchers to focus on those energy resources which are efficient, environment-friendly and cost-effective [1]. So far, fossil fuels are considered the major contributor to fulfilling the needs of energy in the world. However, they have some harmful impacts on the environment, which will cause greenhouse effects and global warming. Therefore, to overcome these limitations, it is necessary to exploit energy resources that emit low carbon than fossil fuels [2,3]. The photovoltaic (PV) based generation is a very suitable choice among the resources described above because of its environment-friendly nature. Moreover, it is free having low maintenance cost [4]. The use of PV panels in the energy sector is growing rapidly with an increase of 30% per year [5]. These PV systems are used, so far, in grid-connected and standalone systems [6]. The PV system portrays nonlinear electrical characteristics, which

depend entirely on atmospheric conditions like solar irradiance [7] and temperature [8]. Variation in these factors changes the power produced from the PV module [9].

Numerous techniques in literature is developed for maximum power extraction from solar system. These techniques are of two types. First is conventional maximum power point tracking (MPPT) algorithms like Perturb and observe (P&O) [10,11] and Incremental Conductance (INC) [12] are mainly used for maximum power extraction from the PV system. In the P&O algorithm, the power difference at different levels of the applied voltage is checked. The applied voltage is perturbed and a change in power is observed. In the perturbation, the increase in power is evaluated with increase/decrease in voltage [13]. Although this is a simple and inexpensive method, however, it has the oscillatory voltage around the point of maximum power extraction rather than steadily staying on it, which is the shortcoming of this method. In the INC method, variation in power with respect to applied voltage is checked, which is denoted by (dP/dV). When $dP/dV = 0$, it means maximum power is extracted. Based on this, the maximum power is calculated in [14] by comparing the incremental conductance denoted by (dI/dV) to the instantaneous conductance expressed by (I/V). In this method, maximum power is extracted with minimum oscillation compare to the P&O process. Still, the main disadvantage of this technique is that it consums more time to reach MPP at some atmospheric conditions [15]. Other conventional techniques reported in the literature are open-circuit voltage (OCV) and short circuit current (SSC) techniques. These techniques are widely used for maximum power extraction because of their inexpensive and straightforward nature. However, these techniques remain ineffective under faster varying environmental conditions [16–18].

In the class of bio-inspired techniques, artificial bee colony [19], particle swarm optimization [20], cuckoo search algorithm [21] and genetic algorithms [22] are commonly used techniques for extraction of maximum power from solar system. These algorithms follow a same scheme or procedure to attain optimization. In the initial step, a population of particles or individuals is produced in the area where the solution exists. These individuals are then randomly initialized to interact with other ones to generate their off springs or new states. The useful solution is obtained by comparing the off springs with their parents via a cost function and the one with good performance than other transforms the new generation. The possibility of attaining the MPP is very good using these techniques as the first population is randomly produced. They show low converging time as compared to the conventional techniques. Moreover, the developed controller effectively controls the system's nonlinearities, making it suitable for resolving the MPPT problem, more often in partial shading conditions. Several parameters like crossover rate, mutation rate, size of the population, chromosome selection are needed in these techniques whose estimation is itself a difficult task. Under abruptly changing atmospheric conditions, these parameters are adjusted with time to track the MPP, otherwise tracking becomes difficult.

Artificial intelligence (AI) based algorithms for maximum power extraction include Artificial Neural Networks (ANN) [23] and Fuzzy Logic Controllers (FLC) [24,25]. These algorithms have advantages like self-learning capabilities, operating with variable inputs and self-converging ability. In the start, the ANN-based method requires a training data set to train the output-input relation, but when it develops, it becomes efficient and robust under abruptly changing input parameters. This method of extracting maximum power has fast-tracking speed and low computation requirement, but they require a large memory size and training to track MPP. In contrast, FLCs do not require mathematical modeling of the system and can handle the system's nonlinear behavior [26,27]. However, its performance and working depends upon the technical information of designer and rule-based tables for tracking and consequently, large memory size in needed.

Different non-linear control techniques are proposed in literature for extraction of maximum power from a PV module like nonlinear backstepping [28] and robust integral backstepping [29]. Backstepping controller is very efficient, but its performance depends on the modeling of a nonlinear system. The system is subjected to variation in time, so the equations use to model the system may vary. Hence the performance of the controller

can be affected. The integral backstepping controller has been found robust and effective in maximum power extraction under abruptly changing meteorological conditions. However, a significant overshoot and steady-state error have been witnessed during the implementation of this controller. Pros and cons of developed and existing techniques are summarized in Table 1. Main challenge that is faced during the implementation of the controller is that the tracking error is needed to converge to zero under the settling time. Moreover, the nonlinear behavior of the PV system is also the major challenge under changing environmental conditions. To resolve the problems state-above, an adaptive nonlinear Sliding Mode Control (SMC) based method is presented, which is insensitive to parameter uncertainties, and internal/external disturbances [30].

Table 1. Explanatory list of the existing control techniques.

Techniques	Advantages	Disadvantages
Conventional	Simple and inexpensive	Oscillatory voltage around the point of maximum power. Time to reach the MPP might be slow under changing conditions.
Bio-inspired	They show low converging time compared to conventional techniques. To resolve the MPPT problems, they are effective in controlling the system's non-linearities	These techniques need many parameters, such as crossover rate, mutation size and chromosome selection, whose estimation is difficult.
Artificial Intelligence (AI)	These techniques have fast tracking speed and low computation requirement.	⊊ Require a large memory size and need more time of training to track MPP.
Nonlinear Controllers	⊊ These techniques are efficient in tracking of MPP. They are robust in extracting maximum power under changing atmospheric conditions.	When implementing these techniques, a significant overshoot and steady-state error has been observed.

In this study, a nonlinear arbitrary order SMC scheme is proposed to collect maximum power from a PV system using DC-DC buck-boost converter. This strategy is illustrated in the Figure 1. With detailed analysis of the overall closed-loop stability, Feed Forward Neural Network (FFNN) is designed to generate peak the desired voltage that is tracked by the proposed control law. In addition, the high gain differentiator is used to observe the system's states, which are utilized by the proposed control algorithm. Results validate the applicability of the developed model for control law in terms of maximum power extraction, steady-state error, and robustness against abrupt variations in atmospheric conditions compared to the conventional MPPT methods. The proposed control strategy finds potential in power applications of PV where one may have PV output from a system with unknown nonlinear dynamics. The proposed control strategy finds potential in power applications of PV where one may have PV output from a system with unknown nonlinear dynamics. The rest of the manuscript is presented in the following structure. In Section 2, an equivalent mathematical model of a PV system is given. Afterward, the detailed modeling of the DC-DC buck-boost converter is provided in Section 3. Section 4 derives the control algorithm for changing duty cycle of buck-boost topology of converter to ensure maximum power extraction. The simulations results are compared with the standered literature results

in Section 5, which endorses robustness of the developed controller. At last, concluding remarks of this work are presented in Section 6.

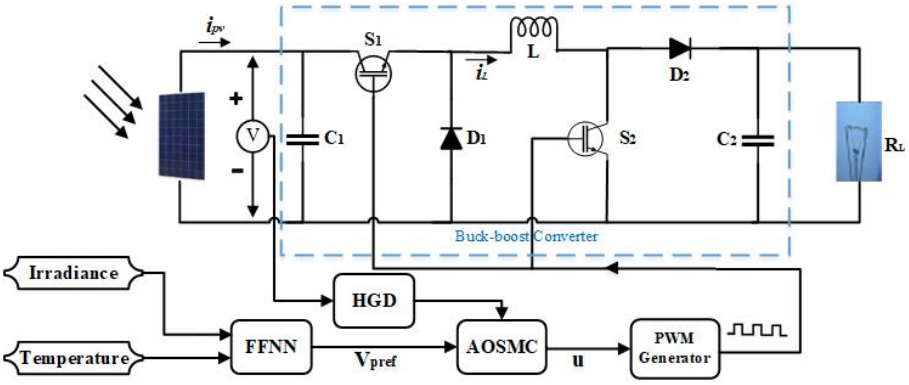

Figure 1. Proposed control methodology.

2. PV System Modeling

A PV system consists of modules that are connected in parallel and series. PV modules are the basic building blocks of a PV system, consisting of a series and parallel combination of PV cells. In general, a single diode model is used for modelling and simulation of a PV system [31,32]. This model is composed of a series resistance R_s, a shunt resistance R_{sh}, a diode D, and a current source I_{ph} (see Figure 2) [33].

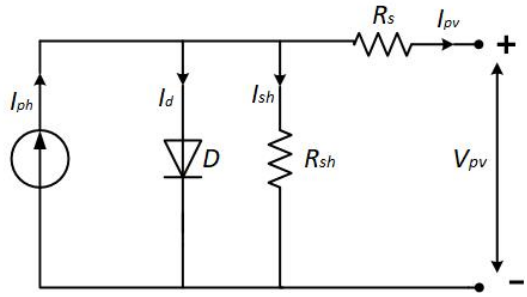

Figure 2. Single diode model of PV system.

PV system I_{pv} represents output current, which is mathematically modeled as

$$I_{pv} = N_p I_{ph} - I_d - I_{sh} \tag{1}$$

where I_sh is the current going through the shunt resistance, I_d is the current travelling through the diode, N_p is the number of parallel linked cells, and I_{ph} is the source current, which is temperature and irradiance dependent.

$$I_{ph} = \left(\frac{G}{G_{ref}}\right)[I_{sc} + K(T - T_{ref})] \tag{2}$$

In the above expression, T signifies temperature, K denotes temperature coefficient, G denotes solar irradiance, and I_{sc} denotes short circuit current at standard solar irradiance G_{ref} and temperature T_{ref}. Shockley's model may be used to obtain the expression for diode current, as shown below.

$$I_d = I_{rs} N_p \left[exp\left(\frac{V_d}{nV_t}\right) - 1\right] \tag{3}$$

where n is the ideality factor of the diode, I_{rs} is the reverse saturation current of the diode, and V_t is the thermal voltage provided by

$$V_t = \left(\frac{kT}{q}\right) \tag{4}$$

where q is the electron charge, T is the temperature and $k = 1.38 \times 10^{-23} J$ is the Boltzmann's constant. The voltage across diode V_d is

$$V_d = \left(\frac{V_{pv} + I_{pv}R_s}{N_s}\right) \tag{5}$$

where V_{pv} denotes the array output voltage, N_s denotes the number of series-connected cells, and R_s is the series resistance. Incorporating (4) and (5) in (3), the expression for diode current becomes

$$I_d = I_{rs}N_p\left[exp\left(\frac{q(V_{pv} + I_{pv}R_s)}{nkN_sT}\right) - 1\right] \tag{6}$$

The current through shunt resistance can be mathematically expressed as

$$I_{sh} = \left(\frac{V_{pv} + I_{pv}R_s}{R_{sh}}\right) \tag{7}$$

Considering (2), (6) and (7), the output current of PV system can be expressed as

$$\begin{aligned} I_{pv} = &\left(\frac{G}{G_{ref}}\right)[I_{sc} + K(T - T_{ref})]N_p - I_{rs}N_p\left[exp\left(\frac{q(V_{pv} + I_{pv}R_s)}{nkN_sT}\right) - 1\right] \\ &- \left(\frac{V_{pv} + I_{pv}R_s}{R_{sh}}\right) \end{aligned} \tag{8}$$

The PV system curves like P-V and I-V are shown in Figures 3 and 4 under varying irradiance and temperature.

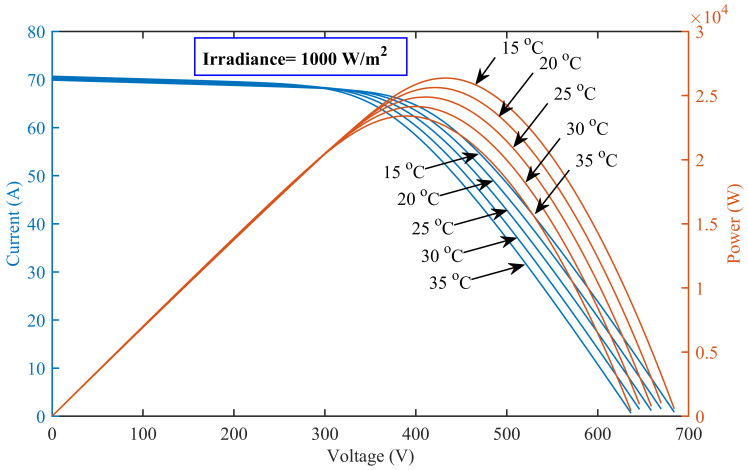

Figure 3. Characteristic curves of P-V and I-V under varying temperature.

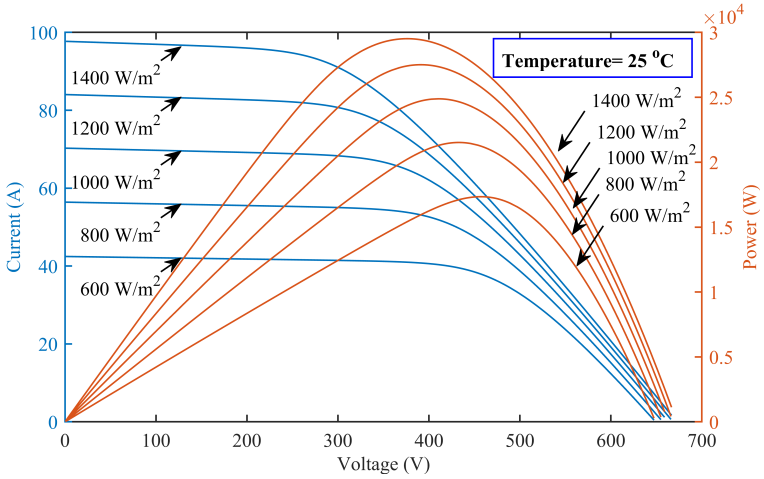

Figure 4. Characteristic curves of P-V and I-V under varying irradiance.

We have modeled the current of the PV system in (8). The non-inverted DC-DC buck-boost topology converter detailed modeling is discussed in subsequent section.

3. Modeling of Non-Inverted DC-DC Buck-Boost Topology of Converter

DC-DC converters are normally used to change the current and voltage level provided by photo voltaic modules that is required by electrical loads [34–36]. The non-inverted DC-DC buck-boost topology of converter [37,38] increase/decrease the output voltage of the PV system in order to get the maximum power point voltage V_{mpp}. To operate the system at V_{mpp}, the converter is controlled periodically by changing its duty cycle with the help of controller proposed in the existing literature. The duty cycle of DC-DC converter is defined as $u = t_{on}/T$, where $T = t_{on} + t_{off}$ shows the total converter time period. Figure 5 depicts converter topology.

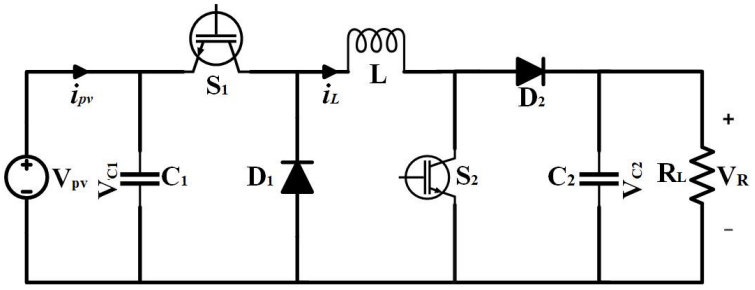

Figure 5. Non-inverted buck boost converter topology.

In Figure 5, V_{pv} represents the input voltage coming from PV system [39]. The input capacitor C_1 is used for limiting the ripples in input voltage of converters. On the other hand, output capacitor C_2 limits the ripples in the converter's output voltage. D_1&D_2 are diodes and S_1&S_2 are Insulated Gate Bipolar Transistors (IGBT) switches. R and L represent the resistor and the inductor of converter, respectively [40]. Before moving into further developments of the converter, the following assumptions are made.

- Diodes and switches are considered ideal, i.e., losses are negligible.
- Converter operation is considered in continuous conduction mode (CCM).
- CCM have two switching intervals in the. The assumption for the first interval is that two switches are turned on, diodes are operating in reverse biased, and the inductor is charging from PV voltage.

Complete discussion of both switching interval is as follows. Applying Kirchoff's laws for the first switching interval, the state space equations can be derived as

$$\begin{bmatrix} \frac{dV_{pv}}{dt} \\ \frac{di_L}{dt} \\ \frac{dV_{C_2}}{dt} \end{bmatrix} = \begin{bmatrix} 0 & -\frac{1}{C_1} & 0 \\ \frac{1}{L} & 0 & 0 \\ 0 & 0 & -\frac{1}{R_L C_2} \end{bmatrix} \begin{bmatrix} V_{pv} \\ i_L \\ V_{C_2} \end{bmatrix} + \begin{bmatrix} \frac{i_{pv}}{C_1} \\ 0 \\ 0 \end{bmatrix} \tag{9}$$

Similarly, apply Kirchoff's laws to find second switching interval using he state space equations, where the load is taken current from the inductor, the diodes are operated in forward biased and both the switches are turned off. The state space equation for this interval is as follows

$$\begin{bmatrix} \frac{dV_{pv}}{dt} \\ \frac{di_L}{dt} \\ \frac{dV_{C_2}}{dt} \end{bmatrix} = \begin{bmatrix} 0 & 0 & 0 \\ 0 & 0 & -\frac{1}{L} \\ 0 & \frac{1}{C_2} & -\frac{1}{R_L C_2} \end{bmatrix} \begin{bmatrix} V_{pv} \\ i_L \\ V_{C_2} \end{bmatrix} + \begin{bmatrix} \frac{i_{pv}}{C_1} \\ 0 \\ 0 \end{bmatrix} \tag{10}$$

The mathematical expression for both switching intervals of non-inverted buck boost topology converter having a resistive load can be presented using the principles of capacitor charge balance and inductor volt-second balance as follows

$$\begin{bmatrix} \frac{dV_{pv}}{dt} \\ \frac{di_L}{dt} \\ \frac{dV_{C_2}}{dt} \end{bmatrix} = \begin{bmatrix} 0 & -\frac{\mu}{C_1} & 0 \\ \frac{\mu}{L} & 0 & \frac{\mu}{L} - \frac{1}{L} \\ 0 & \frac{1}{C_2} - \frac{\mu}{C_2} & -\frac{1}{R_L C_2} \end{bmatrix} \begin{bmatrix} V_{pv} \\ i_L \\ V_{C_2} \end{bmatrix} + \begin{bmatrix} \frac{i_{pv}}{C_1} \\ 0 \\ 0 \end{bmatrix} \tag{11}$$

The output load voltage V_R of non-inverted DC-DC buck boost topology converter is computed as

$$V_R = \frac{\mu}{1-\mu} V_{pv} \tag{12}$$

Considering the ideal power transfer $P_{pv} = P_R$ and eliminating the losses, the relationship between output impedance R and the input impedance R_{pv} is computed using (13)

$$R_{pv} = (\frac{1-\mu}{\mu})^2 R \tag{13}$$

Assuming the average values for V_{pv}, i_L, V_{C2} and μ as x_1, x_2, x_3 and u, respectively, the final state space representation looks like

$$\begin{bmatrix} \dot{x_1} \\ \dot{x_2} \\ \dot{x_3} \end{bmatrix} = \begin{bmatrix} 0 & -\frac{u}{C_1} & 0 \\ \frac{u}{L} & 0 & \frac{u}{L} - \frac{1}{L} \\ 0 & \frac{1}{C_2} - \frac{u}{C_2} & -\frac{1}{R_L C_2} \end{bmatrix} \begin{bmatrix} x_1 \\ x_2 \\ x_3 \end{bmatrix} + \begin{bmatrix} \frac{i_{pv}}{C_1} \\ 0 \\ 0 \end{bmatrix} \tag{14}$$

We have modeled the PV system accompanied by the non-inverting DC-DC converter, which extract maximum power when operates. Therefore, in the forthcoming sections, a control algorithm will be designed for changing duty cycle to meet the maximum power extraction.

4. Proposed Control Strategy for Maximum Power Extraction

Primary objective of the proposed research work is that the output voltage V_{pv} of a non-inverted buck-boost converter should trace a reference voltage V_{ref}. The V_{ref} is characterized as the maximum power obtained at each of its points. So, the maximum power from the actual system can be extracted by tracking the V_{ref}. Reference voltage Tracking is achieved via continuously varying duty cycle u of converter using an output feedback controller.

The proposed control law needs the V_{ref} values, which will be estimated via FFNN in the presence of varying temperature and irradiance. In addition, the controller also uses the

inductor current x_2 as a known data, which is generally not available in a practical scenario. Therefore, an appropriate states estimator along with flatness property is proposed in this research. In the later part, we will focus on the arbitrary order sliding mode control strategy. So, we proceed further by designing FFNN for reference voltage generation.

4.1. Reference Voltage Trajectory via FFNN

The objective is to estimate V_{ref} while considering the environmental parameters, i.e., temperature and irradiance as an input to the FFNN block [41]. For this task, a two-layer feed forward neural network is used, whose schematic diagram is shown in Figure 6. The input data is generated by varying the irradiance (first network input) from (600–1000) W/m^2 with a suitable increment of 1 W/m^2 and changing the temperature (second network inputs) during 25°C–75°C interval with an increment of 2 degree Celsius, accordingly. Based on these available inputs, the inputs (or activation) to the next layer are computed using (15)

$$a_j = \sum_{i=1}^{n} V_{ji} p_i + b_{jo} \tag{15}$$

where p_i is input of node i, b_{jo} represents respective reconstruction bias/error and $j = 1, 2, 3..., jo$ shows number of hidden layer neurons.

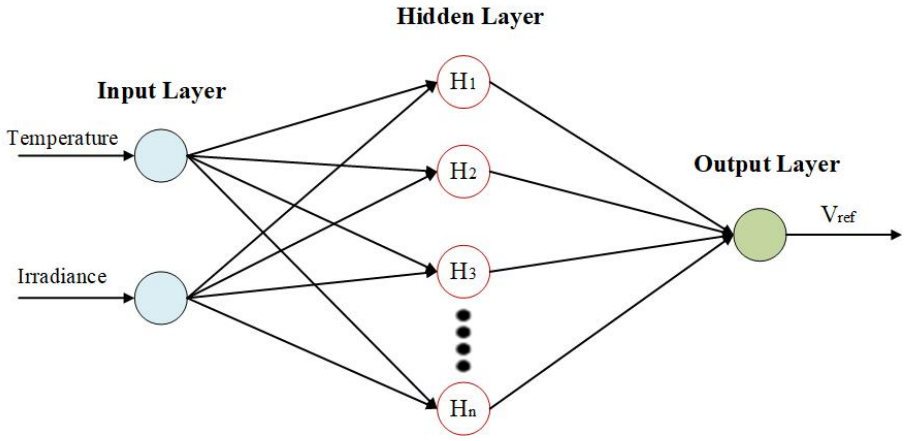

Figure 6. Structure of FFNN for V_{ref} generation.

The outputs of the activation function f (chosen as tanh) at the hidden layer, while invoking a_j, appears as follows

$$y_i = f(a_j) \tag{16}$$

Similarly, the weights in the next layer are named as w_{kj} (w_{kj} is a scalar and is a weight between the j^{th} hidden layer node) and the k^{th} output layer node with y_i as inputs from the hidden layer on which the activation of the output layer will be operated looks like

$$a_k = \sum_{j=1}^{l_o} w_{kj} y_i + b_{ko} \tag{17}$$

where $k = 1$ represents number of neurons in output layer. Estimated V_{ref} output voltage, a function of inputs and weights between hidden layer and output layer is expressed as follows

$$V_{ref} = f(a_k) \tag{18}$$

or

$$V_{ref} = f\left(\sum_{j=1}^{l_o} w_{kj} f\left(\sum_{i=1}^{n} V_{ji} p_i + b_{jo} \right) + b_{ko} \right) \tag{19}$$

Equation (19) can be alternatively expressed in vector form as

$$V_{ref} = \bar{f}\left(\bar{W}^T \bar{f}\left(\bar{V}^T \bar{p} + b_v\right) + b_w\right) \tag{20}$$

Equation (20) can be more explicitly written as

$$V_{ref} = \left(W tanh\left(V\bar{p} + b_v\right) + b_w\right) \tag{21}$$

There is a maximum voltage level on a PV module characteristic curve for each temperature and irradiance level. This maximum voltage is considered as the desired V_{ref} which is the target data during the training of FFNN. The training technique used for updating the weights of a neural network at each iteration is the Levenberg-Marquardt training algorithm.

FFNN Simulation Results

The network parameters used for the estimation of V_{ref} are iterations and hidden layer neurons. The final structure of FFNN has ten neurons in hidden layer. The desired V_{ref} for different values of temperature and irradiance produced from the FFNN in 3-D plane is illustrated in Figure 7. The training of NN is calculated using Mean Squared Error (MSE) depicted in Figure 8. There is a significant amount of error at the start, but the error reduces to the minimum possible value as the number of epochs increases.

The best training performance with the lowest MSE is 1.0836×10^{-6} at 1000 epochs. The regression graph for V_{ref} estimation is given in Figure 9. It shows that the regression value of $R = 1$ indicates the close resemblance of the output data with the target data. The error histogram is calculated with 20 vertical bins. Figure 10 depicts the estimation error histogram associated with V_{ref}, which reveals that a very small error occurs and is nearly close to zero.

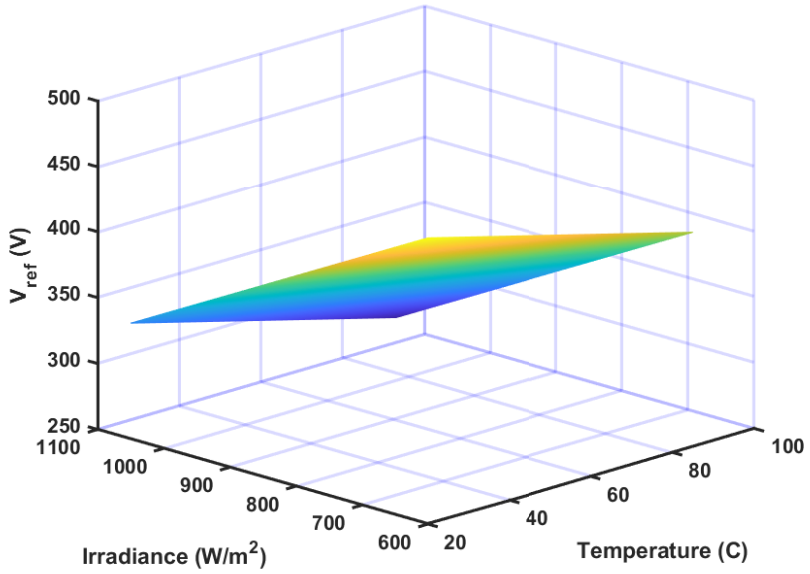

Figure 7. V_{ref} generation for varying level of irradiance and temperature.

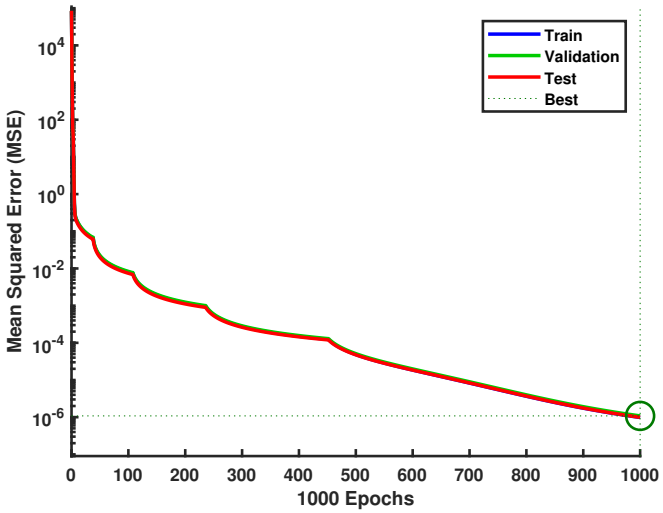

Figure 8. Mean squared error during FFNN estimation.

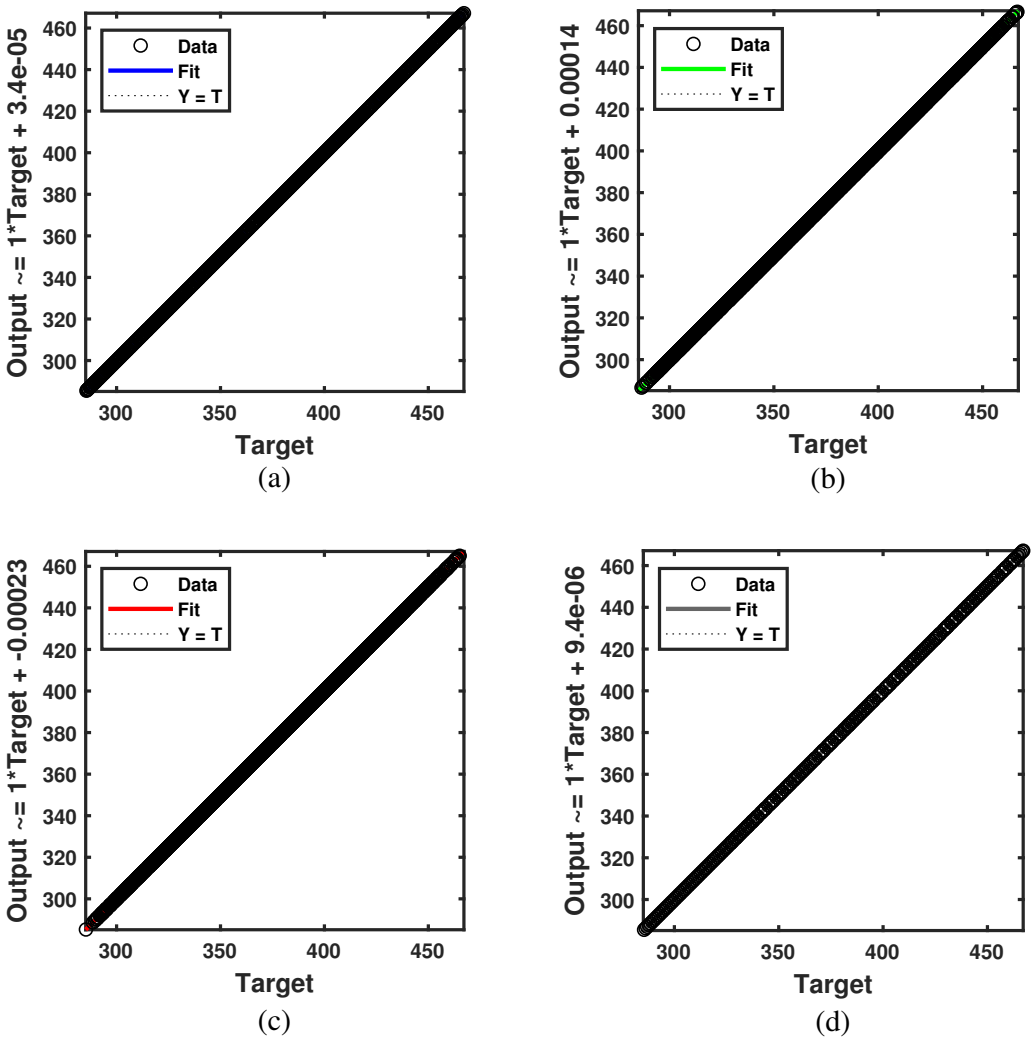

Figure 9. Regression graph (**a**) Training R = 1; (**b**) Validation R = 1; (**c**) Test R = 1; (**d**) All R = 1.

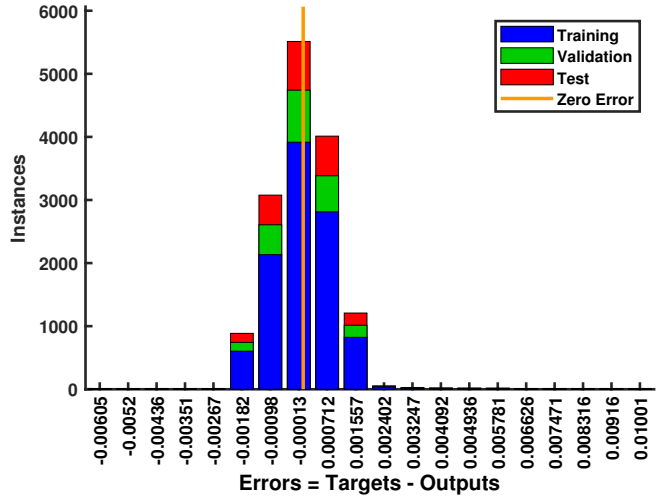

Figure 10. The error histogram with 20 bins.

4.2. Arbitrary Order Sliding Mode Control Design

In this section, a NAAOSMC technique is proposed to obtain maximum power from the PV module. The output of the controller u controls duty cycle of switches of DC-DC converter. For designing the control strategy, the system (14) is converted in canonical form as

$$\begin{cases} \dot{y}_1 = y_2 \\ \dot{y}_2 = \frac{\dot{i}_{pv}}{C_1} - u\frac{\dot{x}_2}{C_1} - \dot{u}\frac{x_2}{C_1} + \Delta(y_1, y_2, t) \end{cases} \tag{22}$$

The system (22) is the controllable canonical form in term of output and its derivative, which is assumed convenient for designing a control strategy. Now, defining tracking error as difference between the reference and maximum PV voltage i.e.,

$$e = y_1 - y_{ref} \tag{23}$$

where $y_{ref} = V_{ref}$ and

$$\begin{aligned} y_1 &= x_1 \\ y_2 = \dot{x_1} &= \frac{i_{pv}}{C_1} - u\frac{x_2}{C_1} \end{aligned} \tag{24}$$

We can achieve our results by converging the tracking error to zero. Taking derivative of (23) and simplify using (24), we get

$$\dot{e} = \frac{i_{pv}}{C_1} - u\frac{x_2}{C_1} - \dot{y}_{ref} \tag{25}$$

As the reference voltage has a fix value so $\dot{y}_{ref} = 0$. Taking derivative of (25)

$$\ddot{e} = \frac{\dot{i}_{pv}}{C_1} - u\frac{\dot{x}_2}{C_1} - \frac{x_2}{C_1}\dot{u} \tag{26}$$

Now, the sliding manifold σ in terms of error is characterized as follows

$$\sigma = \dot{e} + \lambda e + \int f(t)dt \tag{27}$$

Here, λ has a constant value and $f(t)$ is a forcing function, which carries following expression for AOSMC

$$f(t) = c_2 \mid \dot{e} \mid^{\alpha_2} sign(\dot{e}) + b_2 \mid \dot{e} \mid^{\beta_2} sign(\dot{e}) + c_1 \mid e \mid^{\alpha_1} sign(e) + b_1 \mid e \mid^{\beta_1} sign(e) \tag{28}$$

Now, taking the time derivative of (27)

$$\dot{\sigma} = \ddot{e} + \lambda \dot{e} + f(t) \tag{29}$$

Now, integrating the values of $\dot{e}$, $\ddot{e}$ and posing $\dot{\sigma} = 0$, we get the following control law equation, which operates dynamics of system on the sliding manifold $\sigma = 0$

$$\dot{u}_{equ} = \frac{1}{x_2}[\dot{i}_{pv} - \dot{x}_2 u + \lambda(i_{pv} - x_2 u) + C_1 f(t)] \tag{30}$$

Since a practical system works during uncertainties, so, equivalent control law given in (30) will not be able to enforce sliding mode. The overall control law which can enforce the sliding manifold is computed as

$$\dot{u} = \dot{u}_{equ} + \dot{u}_d \tag{31}$$

where $\dot{u}_d$ is given by

$$\dot{u}_d = -k_1 \sigma - k_2 sign(\sigma) \tag{32}$$

Here, k_1 and k_2 are positive gain constants.

Stability Analysis

The objective here is to prove the zero dynamic stability of the system. AOSMC law has been designed using dynamics of first two equations of the system (14). The dynamics of the third equation of the system (14) is clearly the internal dynamics of the given PV system i.e.,

$$\dot{x}_3 = (\frac{1}{C_2} - \frac{u}{C_2})x_2 - \frac{1}{R_L C_2} x_3 \tag{33}$$

Since, the control input u directly affects control driven states like x_1 and x_2 therefore, zero dynamics of a system can be achieved by putting $u = x_1 = x_2 = 0$. So, one can get

$$\dot{x}_3 = -\frac{1}{R_L C_2} x_3 \tag{34}$$

Since, the typical parameters R_L and C_2 are positive, which ensures that the (34) has its poles in the left half-plane at $-\frac{1}{R_L C_2}$. This shows that the system (34) has exponentially stabilized the zero dynamics and validated the PV system's minimum phase nature. Furthermore, to ensure sliding mode enforcement, a Lyapunov stability function in aspects sliding surface is chosen and modeled as

$$V = \frac{1}{2}\sigma^2 \tag{35}$$

Taking time derivative of Equation (35), we can get

$$\dot{V} = \sigma \dot{\sigma} \tag{36}$$

Now, incorporating the components of (30) and (32), we can get

$$\dot{V} = \sigma \left[-\frac{x_2}{C_1} k_1 \sigma - \frac{x_2}{C_1} k_2 sign(\sigma) + \Delta \right] \tag{37}$$

$$\dot{V} = -\frac{x_2}{C_1}k_1\sigma^2 - \frac{x_2}{C_1}\sigma k_2 sign(\sigma) + \sigma\Delta \tag{38}$$

or

$$\dot{V} \leq -\frac{x_2}{C_1}k_1\sigma^2 - \frac{x_2}{C_1}k_2|\sigma| + |\sigma||\Delta| \tag{39}$$

$$\dot{V} \leq -\frac{x_2}{C_1}k_1\sigma^2 - |\sigma|(\frac{x_2}{C_1}k_2 - |\Delta|) \tag{40}$$

(40) becomes negative definite, when

$$\frac{x_2}{C_1}k_2 - |\Delta| \geq \eta \tag{41}$$

From (40) and (41), one can write

$$\dot{V} \leq -\frac{x_2}{C_1}k_1 2V - \sqrt{2}\eta V^{\frac{1}{2}} \tag{42}$$

or

$$\dot{V} + \frac{x_2}{C_1}k_1 2V + \sqrt{2V}\eta \leq 0 \tag{43}$$

The differential inequality of (43) demonstrates a finite-time convergence, forcing the function V approaches to zero, i.e., $\sigma \to 0$. It ensures that the sliding mode is established and the error is converged to zero.

4.3. States Estimation via High Gain Differentiator

State estimation is the process that deals with estimating the internal states of a real system with its perspective outputs. This process also involves the reduction of chattering effect from the input signal. The method used for states estimation in this paper is High Gain Differentiator (HGD). HGD is quite useful in estimating the derivatives of the states (x_1, x_2, x_3, I_{pv}) of the given PV system. The equations for HGD [42] to estimate derivative of the states of the system are

$$\dot{y_1} = y_2 + \frac{\alpha_1}{\epsilon}(x_1 - y_1) \tag{44}$$

$$\dot{y_2} = \frac{\alpha_2}{\epsilon^2}(x_1 - y_1) \tag{45}$$

where $0 < \epsilon < 1$ and α_1, α_2 are gains of HGD.

The HGD technique used for estimating the derivatives of the system states is used further by invoking flatness property for recovery of the unknown states.

Definition 1. *A flat system is defined as the system whose states/parameters/inputs can be expressed in terms of the flat outputs and their derivatives, For example*

$$x_j = \Phi(x_i, \dot{x}_i, ..., x_k, \dot{x}_k, ..., u, \dot{u}, ...u_r) \tag{46}$$

where $x_i, \dot{x}_i, x_k, \dot{x}_k, u, \dot{u}, u_r$ are the states and the derivatives of the system's variables.

In general, the measurement of x_2 is not available, therefore, using HGD and the flatness property, one can estimate the value of x_2 as

$$x_{2(e)} = -\frac{C_1}{u}(\dot{x_1} - \frac{I_{pv}}{C_1}) \tag{47}$$

5. Simulation Results and Discussion

The simulation results are performed using Simulink environment of MATLAB (R2018b) environment to check the applicability of the developed HGD based AOSMC. The solar array system is connected with load using DC-DC buck-boost converter. Solar

array system used for the simulation in this study has 16 PV modules. The specification parameters of a single PV module are given in Table 2 and the specification of the buck-boost converter and designed constants of the proposed controller are listed in Table 3. Section 5 results are presented and discussed into two sections. The results under varying irradiance levels are given in Section 5.1 and results under varying temperature levels are shown in Section 5.2.

Table 2. Parameters of solar panels.

Parameters	Value	Unit
No. of cells per module	72	–
Open circuit voltage	165.8	V
Short circuit current	17.56	A
Max. power	1555	W
Voltage at MPP	102.6	V
Current at MPP	15.16	A

Table 3. MATLAB simulation parameters.

Parameters	Value	Unit
Constant	$c_2 = 0.005$	–
Constant	$b_2 = 0.003$	–
Gain	$k_1 = 3000$	–
Gain	$k_2 = 10$	–
Constant	$c_1 = 0.3$	–
Constant	$b_1 = 0.5$	–
Output capacitor	$C_2 = 48$	mF
Input capacitor	$C_1 = 1$	mF
Inductor	$L = 1.5$	mH
Load	$R_L = 50$	Ω

5.1. Results under Varying Irradiance

To perform imulation for varying irradiance levels, the temperature was kept constant at 25 °C, and the irradiance was changed as shown in Figure 11. The generated reference voltage V_{ref} using FFNN for changing irradiance profile was tracked by the proposed AOSMC. It can be seen from Figure 12 that the V_{ref} was effectively obtained using our developed controller in 0.01 s with a slight overshoot of 3 V. Similarly, in Figure 13, the PV system output power is presented with reference power curves as a result of varying irradiance levels, which depicts that the MPP was attained with minor oscillations and in a short time of 0.02 s.

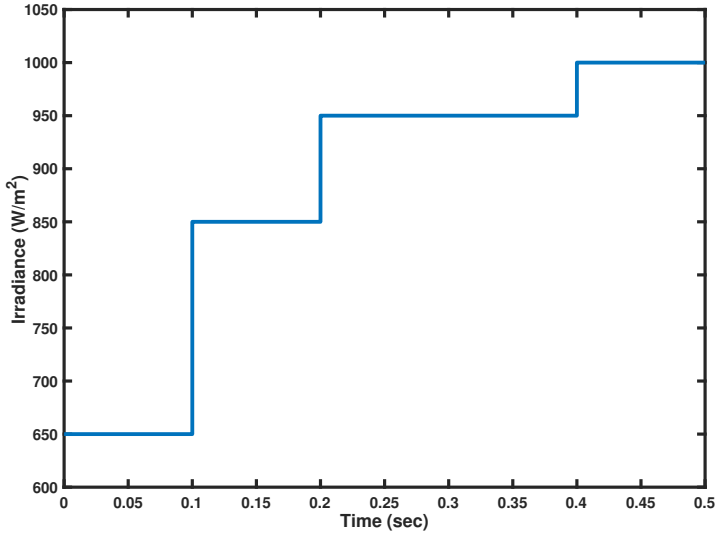

Figure 11. Varying levels of irradiance.

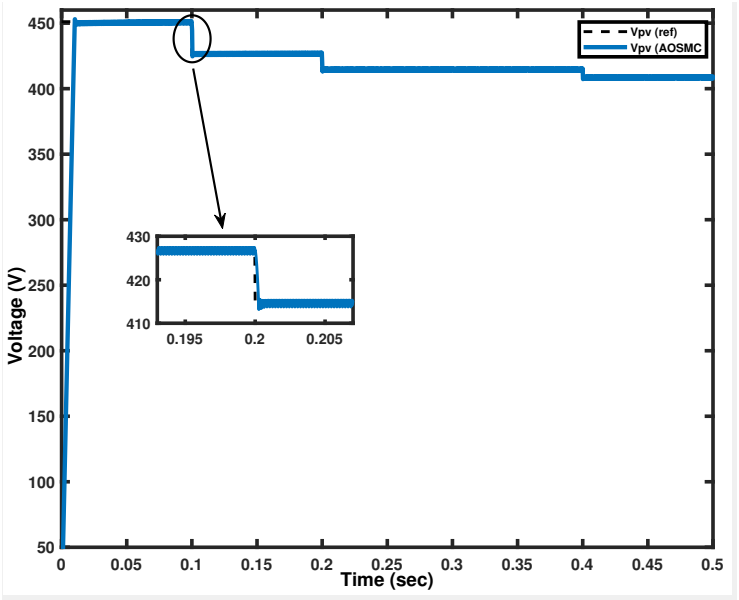

Figure 12. Tracking the PV voltage under varying irradiance.

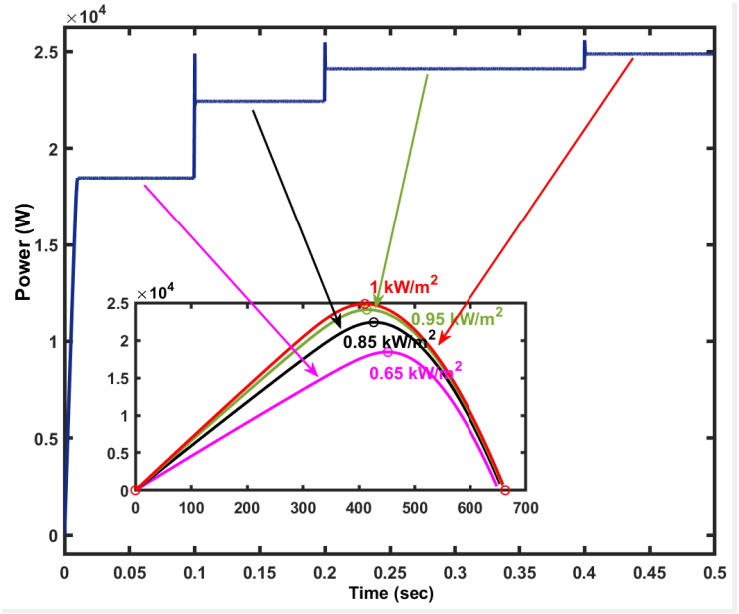

Figure 13. PV output power under varying irradiance.

5.2. Results under Varying outdoor Temperature

In this case, if solar irradiance is maintain fixed i.e., 1000 W/m^2, and outdoor temperature is continuously changed, the obtained observations are depicted in Figure 14. It is clearly seen in the Figure that generated voltage from FFNN with changing outdoor temperature profile is successfully tracked using the developed AOSMC. However, an overshoot of 7 V was observed (See Figure 15). Similarly, for varying temperature levels, the PV system output power is presented in Figure 16, which portrays that the maximum power was obtained in 0.01 s without oscillations.

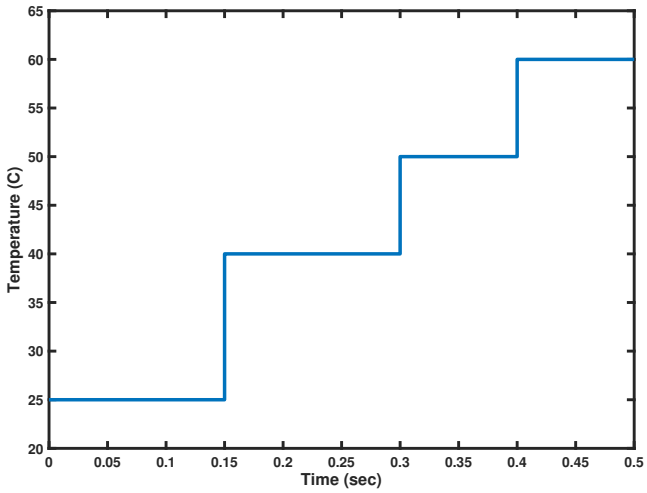

Figure 14. Varying levels of temperature.

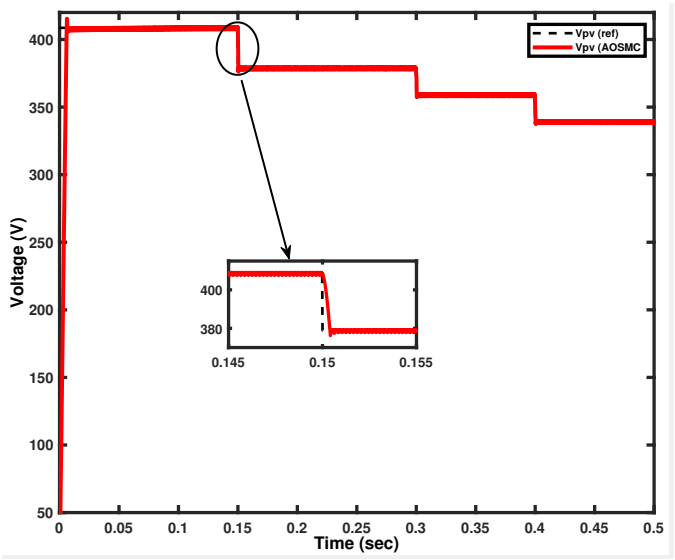

Figure 15. Voltage tracking in PV system under varying temperature conditions.

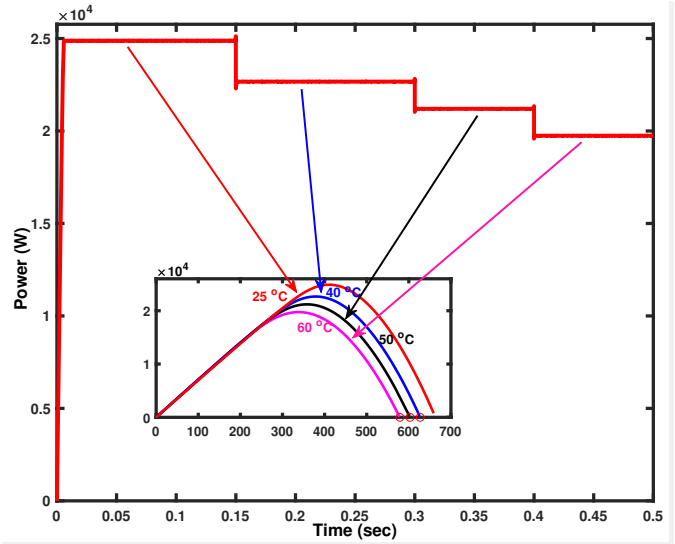

Figure 16. The PV output power under varying temperature.

From both of the above cases, it is evident that the proposed AOSMC can extract the maximum power, which is transmitted with 98 % efficiency to load under changing temperature and irradiance levels. To evaluate performance of the developed controller, the backstepping controller [26] is considered as a benchmark under similar changing conditions.

5.3. Comparison Results under Varying Irradiance

Comparative evaluation of the developed controller with the backstepping controller was made as shown in Figure 17 using similar irradiance variation as given in Figure 11. We observed that the proposed controller tracked the MPP in 0.01 s, whereas the backstepping controller attained this in 0.025 s (see the zoomed view in Figure 17). It can also be noted that the developed controller's rise time was 0.002 s, which is less than the backstepping controller. The comparison of solar array system output power is depicted in Figure 18, which portrays that the proposed AOSMC had less power loss and was 5 % more efficient than the backstepping controller.

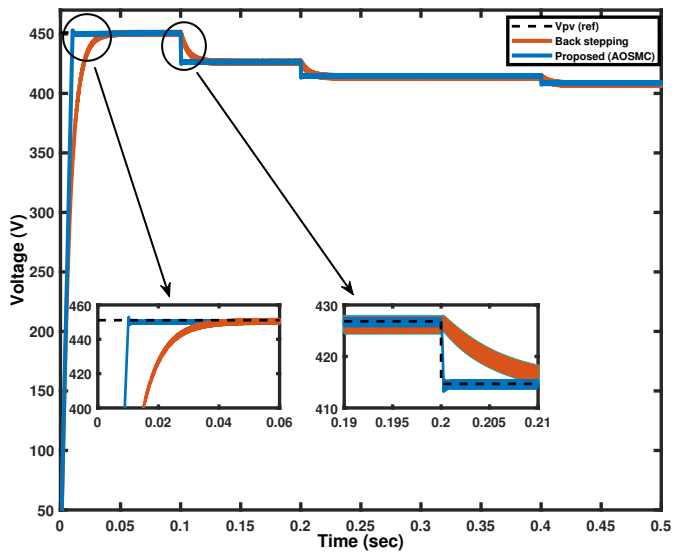

Figure 17. Comparison of voltage in PV system under varying irradiance.

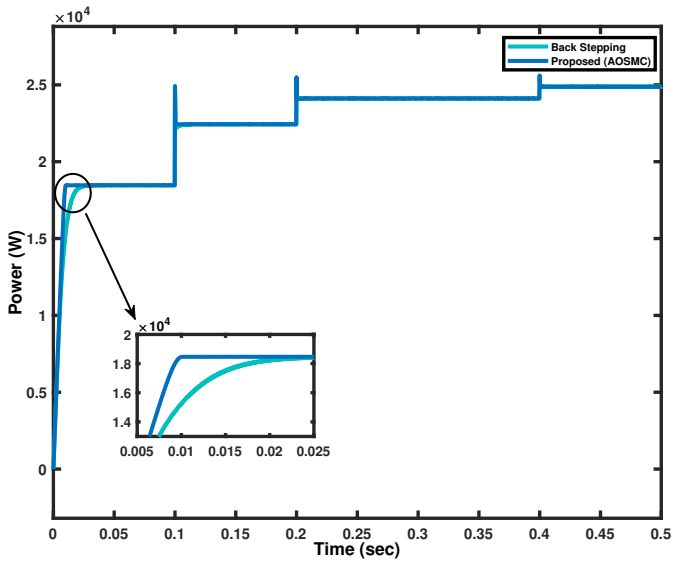

Figure 18. Comparison of the generated output power under varying irradiance.

5.4. Comparison Results under Varying Temperature

In this case, using the similar temperature variation of Figure 14, a comparison was made between the proposed AOSM controller and the backstepping controller as displayed in Figure 19. The figure depicts that the proposed controller extracted the maximum power in 0.01 s, which was 0.02 s in the case of the backstepping controller during the changing temperature levels. The solar array system output power comparison of both controllers is shown in Figure 20. The proposed AOSMC transmit maximum power with 97% efficiency to load, and thus outperformed the existing backstepping controller.

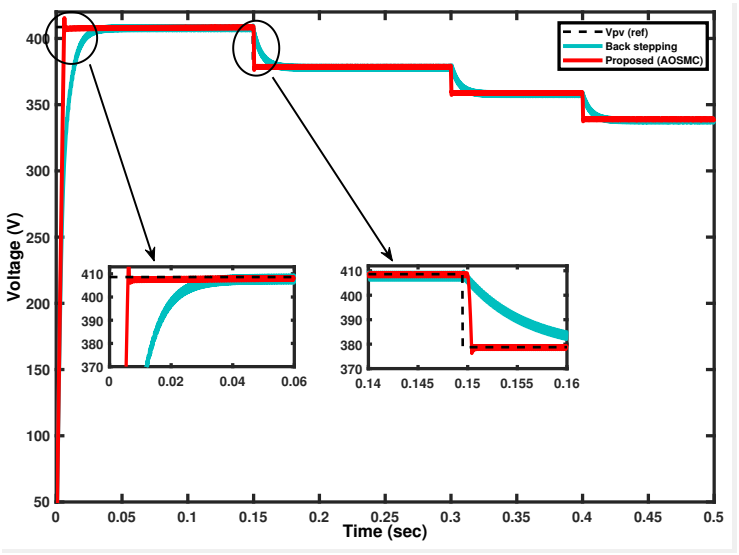

Figure 19. Comparison of voltage PV system under varying temperature.

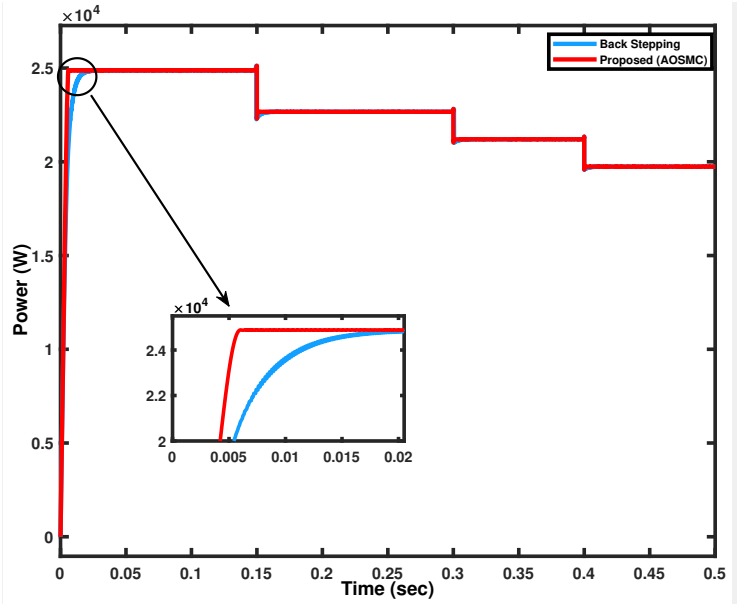

Figure 20. Comparison of the generated output power under varying temperature.

6. Conclusions

In this article, we proposed an HGD-based arbitrary order sliding mode nonlinear MPPT control design for a PV system. The PV module was connected to the load using a non-inverting DC-DC buck-boost converter. FFNNs were used to produce the reference voltage. After developing the reference voltage, the proposed controller was used to track the reference voltage. HGD technique was used to estimate the internal states of the system.

The observer also used the flatness property to recover the non-observable state. The simulation results were performed in Simulink environment of MATLAB, which shows that the proposed controller performed well under changing atmospheric conditions. Simulation results of AOSMC were compared with the backstepping control technique results under abrupt variations in temperature and irradiance. The results verify that the AOSMC outperformed the existing backstepping controller. Hence, we can conclude that the proposed controller was validated for efficiency and effectiveness with improved robustness.

Author Contributions: Conceptualization, M.B.A., Q.K., G.H. and F.R.A.; Data curation, Q.K. and G.H.; Formal analysis, Q.K., S.U., G.H., J.I. and F.R.A.; Funding acquisition, S.U., G.H., J.I. and F.R.A.; Investigation, M.B.A., Q.K. and G.H.; Methodology, M.B.A., Q.K., S.U., G.H., A.F. and F.R.A.; Project administration, Q.K., G.H., A.F. and F.R.A.; Resources, S.U. and G.H.; Software, Q.K. and G.H.; Supervision, Q.K., G.H. and A.F.; Validation, M.B.A. and G.H.; Visualization, M.B.A. and G.H.; Writing—original draft, M.B.A. and S.U.; Writing—review & editing, M.B.A., Q.K., S.U., G.H., A.F., J.I. and F.R.A. All authors have read and agreed to the published version of the manuscript.

Funding: The APC is funded by Taif University Researchers Supporting Project Number(TURSP-2020/331), Taif University, Taif, Saudi Arabia.

Institutional Review Board Statement: Not applicable.

Informed Consent Statement: Not applicable.

Data Availability Statement: Not applicable.

Acknowledgments: The authors would like to acknowledge the support from Taif University Researchers Supporting Project Number(TURSP-2020/331), Taif University, Taif, Saudi Arabia.

Conflicts of Interest: The authors declare no conflict of interest.

References

1. Irfan, M.; Iqbal, J.; Iqbal, A.; Iqbal, Z.; Riaz, R.A.; Mehmood, A. Opportunities and challenges in the control of smart grids-Pakistani perspective. *Renew. Sustain. Energy Rev.* **2017**, *71*, 652–674.
2. Mohamed, M.A.; Eltamaly, A.M.; Alolah, A.L. PSO-based smart grid application for sizing and optimization of hybrid renewable energy systems. *PLoS ONE* **2016**, *11*, e0159702.
3. Iqbal, J.; Khan, Z.H. The potential role of renewable energy sources in robot's power system: A case study of Pakistan. *Renew. Sustain. Energy Rev.* **2017**, *75*, 106–122.
4. Reisi, A.R.; Moradi, M.H.; Jamasb, S. Classification and comparison of maximum power point tracking techniques for photovoltaic system: A review. *Renew. Sustain. Energy Rev.* **2013**, *19*, 433–443.
5. Pandya, R.; Vardia, M. Grid-connected PV system with MPPT control and P&O technique. *Int. J. Adv. Res. Innov. Ideas Educ.* **2016**, *2*, 530–534
6. Zhou, S.; Kang, L.; Sun, J.; Guo, G.; Cheng, B.; Cao, B.; Tang, Y. A novel maximum power point tracking algorithms for standalone photovoltaic system. *Int. J. Control Autom. Syst.* **2011**, *8*, 1364–1371.
7. Jena, S.; Sahoo, S.; Panigrahi, C.K. Effect of irradiance onyield factor of solar photovoltaic plant-A case study. In Proceedings of the 2017 International Conference on Innovative Mechanisms for Industry Applications (ICIMIA), Bangalore, India, 21–23 February 2017; pp. 597–601.
8. Razak, A.; Yusoff, M.I.; Zhe, L.W.; Irwanto, M.; Ibrahim, S.; Zhafarina, M. Investigation of the Effect Temperature on Photovoltaic (PV) Panel Output Performance. *Int. J. Adv. Sci. Eng. Inf. Technol.* **2016**, *6*, 682–688.
9. Martin, A.D.; Cano, J.M.; Silva, J.F.; Vazquez, J.R. Backstepping Control of Smart Grid-Connected Distributed Photovoltaic Power Supplies for Telecom Equipment. *IEEE Trans. Energy Convers.* **2015**, *30*, 1496–1504.
10. Kollimalla, S.K.; Mishra, M.K. Variable Perturbation Size Adaptive P&O MPPT Algorithm for Sudden Changes in Irradiance. *IEEE Trans. Sustain. Energy* **2014**, *5*, 718–728.
11. Bhatnagar, P.; Nema, R. Maximum power point tracking control techniques: State-of-the-art in photovoltaic applications. *Renew. Sustain. Energy Rev.* **2013**, *23*, 224–241.
12. Loukriz, A.; Haddadi, M.; Messalti, S. Simulation and experimental design of a new advanced variable step size Incremental Conductance MPPT algorithm for PV systems. *ISA Trans.* **2016**, *62*, 30–38.
13. Subudhi, B.; Pradhan, R. A Comparative Study on Maximum Power Point Tracking Techniques for Photovoltaic Power Systems. *IEEE Trans. Sustain. Energy* **2013**, *4*, 89–98.
14. Elgendy, M.A.; Zahawi, B.; Atkinson, D.J. Assessment of the Incremental Conductance Maximum Power Point Tracking Algorithm. *IEEE Trans. Sustain. Energy* **2013**, *4*, 108–117.

15. Cristaldi, L.; Faifer, M.; Rossi, M.; Toscani, S. An Improved Model-Based Maximum Power Point Tracker for Photovoltaic Panels. *IEEE Trans. Instrum. Meas.* **2014**, *63*, 63–71.
16. Das, P. Maximum Power Tracking Based Open Circuit Voltage Method for PV System. *Energy Procedia* **2016**, *90*, 2–13.
17. Kamarzaman, N.A.; Tan, C.W. A comprehensive review of maximum power point tracking algorithms for photovoltaic systems. *Renew. Sustain. Energy Rev.* **2014**, *37*, 585–598.
18. Masoum, M.A.; Dehbonei, H.; Fuchs, E.F. Theoretical and experimental analyses of photovoltaic systems with voltage and current-based maximum power-point tracking. *IEEE Trans. Energy Convers.* **2002**, *17*, 514–522.
19. Banyoucef, A.S.; Chouder, A.; Kara, K.; Silvestre, S.; Sahed, O.A. Artificial bee colony based algorithm for maximum power point tracking (MPPT) for PV systems operating under partial shaded conditions. *Appl. Soft Comput.* **2015**, *32*, 38–48.
20. Liu, Y.H.; Huang, S.C.; Huang, J.W.; Liang, W.C. A Particle Swarm Optimization-Based Maximum Power Point Tracking Algorithm for PV Systems Operating Under Partially Shaded Conditions. *IEEE Trans. Energy Convers.* **2012**, *27*, 1027–1035.
21. Ahmed, J.; Salam, Z. A Maximum Power Point Tracking (MPPT) for PV system using Cuckoo Search with partial shading capability. *Appl. Energy* **2014**, *119*, 118–130.
22. Daraban, S.; Petreus, D.; Morel, C. A novel MPPT (maximum power point tracking) algorithm based on a modified genetic algorithm specialized on tracking the global maximum power point in photovoltaic systems affected by partial shading. *Energy* **2014**, *74*, 374–388.
23. Liu, Y.H.; Liu, C.L.; Huang, J.W.; Chen, J.H. Neural-network-based maximum power point tracking methods for photovoltaic systems operating under fast changing environments. *Sol. Energy* **2013**, *89*, 42–53.
24. Bounechba, H.; Bouzid, A.; Nebti, K.; Benalla, H. Comparison of Perturb & Observe and Fuzzy Logic in Maximum Power Point Tracker for PV Systems. *Energy Procedia* **2014**, *50*, 677–684.
25. Guenounou, O.; Dahhou, B.; Chabour, F. Adaptive fuzzy controller based MPPT for photovoltaic systems. *Energy Convers. Manag.* **2014**, *78*, 843–850.
26. Ullah, S.; Khan, Q.; Mehmood, A.; Kirmani, S.A.M.; Mechali, O. Neuro-adaptive fast integral terminal sliding mode control design with variable gain robust exact differentiator for under-actuated quadcopter UAV. *ISA Trans.* 2021, *in Press*.
27. Ullah, S.; Khan, Q.; Mehmood, A.; Bhatti, A.I. Backstepping based sliding mode control for a class of under-actuated electro-mechanical nonlinear systems: Application to the cart-pendulum. *J. Electr. Eng. Technol.* **2020** *15*, 1821–1828.
28. Naghmash, Armghan, H.; Ahmad, I.; Armghan, A.; Khan, S.; Arsalan, M. Backstepping based nonlinear control for maximum power point tracking in photovoltaic system. *Sol. Energy* **2018**, *159*, 134–141.
29. Ali, K.; Khan, L.; Khan, Q.; Ullah, S.; Ahmad, S.; Mumtaz, S.; Karam, F.W.; Naghmash. Robust Integral Backstepping Based Nonlinear MPPT Control for a PV System. *Energies* **2019**, *12*, 3180–3199.
30. Ullah, S.; Mehmood, A.; Khan, Q.; Rehman, S.; Iqbal, J. Robust Integral Sliding Mode Control Design for Stability Enhancement of Under-actuated Quadcopter. *Int. J. Control Autom. Syst.* **2020**, *18*, 1671–1678.
31. Muhammad, F.F.; Yahya, M.Y.; Hameed, S.S.; Aziz, F.; Sulaiman, K.; Rasheed, M.A.; Ahmad, Z. Employment of single-diode model to elucidate the variations in photovoltaic parameters under different electrical and thermal conditions. *PLoS ONE* **2017**, *12*, e0182925.
32. Bellia, H.; Youcef, R.; Fatima, M. A detailed modeling of photovoltaic module using MATLAB. *NRIAG J. Astron. Geophys.* **2014**, *3*, 53–61.
33. Roslan, M.F.; Al-Shtewi, A.Q.; Hannan, M.A.; Ker, P.J.; Zuhdi, A.W.M. Particle swarm optimization algorithm-based PI inverter controller for a grid-connected PV system. *PLoS ONE* **2020**, *15*, e0243581.
34. Arango, E.; Ramos-Paja, C.A.; Calvente, J.; Giral, R.; Serna-Garces, S.I. Asymmetrical Interleaved DC/DC switching converters for photovoltaic and fuel cell applications-part 2: Control-oriented models. *Energies* **2013**, *6*, 5570–5596.
35. Robles-Algarin, C.; Hernandez, D.S.; Viloria-Porto, Y.J. Design and implementation of a four switch buck-boost converter for off-grid pv applications. *Int. J. Energy Convers.* **2020**, *8*, 190–199
36. Omar, M.A.; Mahmoud, M. Design and simulation of DC/DC boost converter with maximum power point tracking for grid connected PV inverter considering the nonlinearity of the PV generator. *Int. J. Energy Convers.* **2019**, *7*, 241–252.
37. Gaboriault, M.; Notman, A. A high efficiency, non-inverting, buck-boost DC-DC converter. In Proceedings of the Annual IEEE Applied Power Electronics Conference and Exposition, Anaheim, CA, USA, 22–26 February 2004; pp. 1411–1415.
38. Shiau, J.-K.; Al-Shtewi, A.Q.; Hannan, M.A.; Ker, P.J.; Cheng, C.-J. Design of a non-inverting synchronous buck-boost DC/DC power converter with moderate power level. *Robot. Comput. Integr. Manuf.* **2010**, *26*, 263–267
39. Selvakumar, S.; Madhusmita, M.; Koodalsamy, C.; Simon, S.P.; Sood, Y.R. High-Speed Maximum Power Point Tracking Module for PV Systems. *IEEE Trans. Ind. Electron.* **2019**, *66*, 1119–1129.
40. Wens, M.; Steyaert, M. *Design and Implementation of Fully-Integrated Inductive DC-DC Converters in Standard CMOS*; Springer Science & Business Media: Berlin/Heidelberg, Germany 2011.
41. Hagan, M.T.; Demuth, H.B.; Beale, M.H.; Jesus, O.D. *Neural Network Design*; PWS Publishing Co.: Boston, MA, USA, 1996; Volume 20.
42. Vesiljevic, L.K.; Khalil, H.K. Differentiation with High-Gain observers the presence of measurement noise. In Proceedings of the 45th IEEE Conference on Decision and Control, San Diego, CA, USA, 13–15 December 2006.